Mixing of the fully symmetric vibrational modes in carbon nanotubes

M. Mohr,* M. Machón, and C. Thomsen
Institut für Festkörperphysik, Technische Universität Berlin, Hardenbergstrasse 36, 10623 Berlin, Germany

I. Milošević and M. Damnjanović
Faculty of Physics, University of Belgrade, P.O. Box 368, 11011 Belgrade, Serbia

(Received 31 October 2006; revised manuscript received 21 February 2007; published 1 May 2007)

We study the mixing of the fully symmetric modes in single-walled carbon nanotubes with *ab initio* calculations. With a variational model, we confirm the results from finite-difference calculations. We further analyze the effect of the mixing on the calculation of phonon frequencies and electron-phonon coupling matrix elements $\mathcal{M}_{e\text{-}ph}$. We find that neglecting the mixing leads to errors of up to 60% for $\mathcal{M}_{e\text{-}ph}$ for the radial breathing mode and up to 50 cm^{-1} difference for the high-energy mode frequency.

DOI: 10.1103/PhysRevB.75.195401 PACS number(s): 61.46.Fg, 71.15.Mb, 63.22.+m, 63.20.Kr

I. INTRODUCTION

The radial breathing mode (RBM) plays a key role in the characterization of carbon nanotubes (NTs). Its diameter-dependent frequency is used in resonant Raman spectroscopy to estimate the nanotube diameter d and for chirality assignments.[1,2] The radial breathing mode is often assumed to be purely radial,[3,4] although several independent studies showed that it has small nonradial components.[5–8] Of similar importance for optical measurements are the high-energy modes (HEMs) around 1600 cm^{-1}, which correspond to the two doubly degenerated optical modes of graphite. Small nontangential components of these eigenvectors have been reported in Ref. 9. Since both the RBM and at least one of the HEMs are fully symmetric, their coupling is not forbidden by symmetry. The large frequency separation (approximately a factor of 8) suggests, though, that the coupling is small. This was first pointed out by Kürti *et al.*,[6] who found slight deviations from the ideal $1/d$ behavior of the RBM frequency, depending on tube chirality and conduction character.

In this paper, we study quantitatively the mixing of the RBM and the HEMs by means of a variational method. We analyze the size and influence of the new small components on phonon frequency calculations, on electron-phonon coupling, and on the analysis of optical spectra of nanotube samples. We find that neglecting the mixing introduces an error of up to 10 cm^{-1} for the RBM frequencies of small tubes. For the electron-phonon coupling matrix elements $\mathcal{M}_{e\text{-}ph}$, we find a startling increase of up to 60% for the RBM. This is of special interest as the intensity I in resonant Raman experiments is proportional to the square of these matrix elements, $I \propto |\mathcal{M}_{e\text{-}ph}|^2$. Neglecting the mixing results in errors for the HEM of up to 50 cm^{-1} in frequency and an increase of a few percent for the electron-phonon coupling matrix elements.

II. METHOD

Our variational density-functional theory approach is based on the fact that an atomic displacement increases the total energy of a nanotube. If we displace all atoms according to a pattern that belongs to an irreducible representation, the direction with extremal value of this energy increase corresponds to a vibrational normal mode. Said another way, for a set of displacement patterns with a given symmetry, the energy has a local extremum when the pattern coincides with a vibrational eigenvector. The same idea was applied in Ref. 10 for nanotubes, but within an oversimplified dynamical model, and in Ref. 11 for benzene.

The displacement pattern was obtained in the following way: One atom of the relaxed nanotube structure was moved on the surface of a sphere centered on the relaxed position of the atom with a fixed radius r. Then, the same symmetry operations that are used to construct the nanotube from one atom (except for mirror operations) were applied to the displacement and the resulting set of displacements was added to the relaxed positions.[12] Thus, the displacement pattern of the whole NT is defined by the displacement of one atom. We define the displacement direction by two parameters φ and ϑ as shown in the inset of Fig. 1 and evaluate the total energy as a function of these parameters. As required by a fully symmetric displacement, all atomic forces are equal within our accuracy.

Ab initio calculations were performed with the SIESTA code[13,14] using the local-density approximation functional in the parametrization of Perdew and Zunger[15] and Troullier-Martins[16] pseudopotentials. An equivalent energy cutoff of 270 Ry was used for the real-space grid integrations and a $(1\times1\times30)$ Monkhorst-Pack[17] mesh in reciprocal space. The valence electrons were described by a double-ζ basis set with cutoff radii of 5.12 and 6.25 bohr for the s and p orbitals, respectively, plus an additional polarizing orbital. The undisplaced coordinates were obtained from relaxing all atoms until all forces were below 0.01 eV/Å.

III. EIGENVECTORS

We scanned the full (ϑ,φ) parameter range for selected nanotubes. The energy $E(\vartheta,\varphi)$ over a half sphere for all nanotubes shows a minimum in the vicinity of $(\vartheta=90°, \varphi=0°)$ and two saddle points close to $(\vartheta=90°, \varphi=-90°)$ and $(\vartheta=180°, \varphi=0°)$ (see Fig. 2 for a full sphere). For achiral tubes, one of the saddle points corresponds to the fully sym-

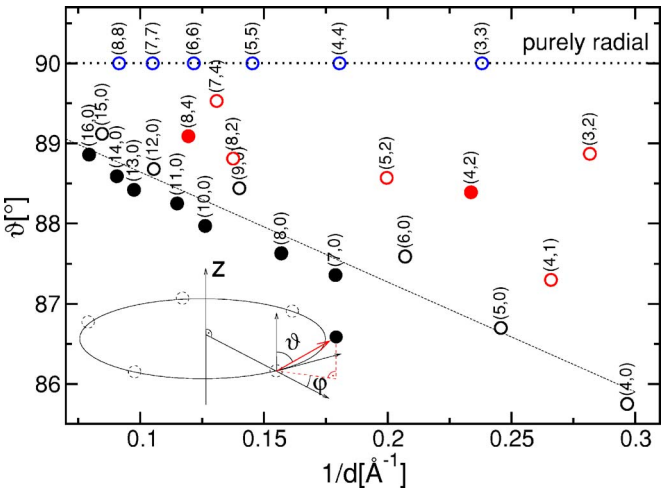

FIG. 1. (Color online) Angle ϑ as function of the inverse nanotube diameter for several nanotubes (open symbols denote metallic, while filled symbols denote semiconducting NTs). The full line shows a linear fit for all zigzag tubes. The metallic $(n,0)$ tubes are above the line, while the semiconducting $(n,0)$ are below. Thus, the RBM is more radial for metallic zigzag tubes than for semiconducting zigzag tubes. Inset: A section of a (5,0) nanotube with five C atoms illustrating the definition of φ and ϑ.

metric HEM and the other to an A_{1u} mode. The HEMs show anharmonicity, also found in calculations of the corresponding graphene modes. The anharmonicity disappears for the A_{1u} mode. This is required by symmetry considerations and makes us confident of the numerical accuracy of our method. For the remainder of this paper, we take care of this anharmonicity by averaging over positive and negative displacements.

For all other NTs, we scanned the vicinity of the point $(\vartheta=90°\ \varphi=0°)$ corresponding to the radial displacement. To obtain the direction of minimal energy, the total-energy values were then fitted to a two-dimensional function of third degree. This fit was used to find the energy minimum $E(\vartheta,\varphi)$ analytically. In the following, we call the position of

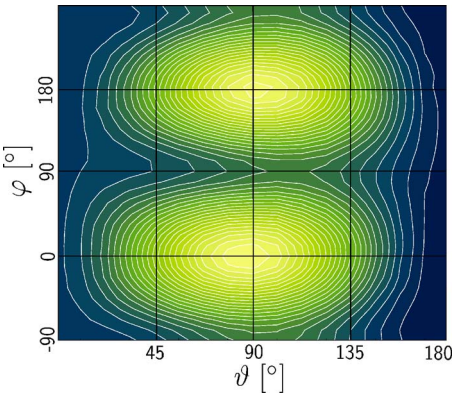

FIG. 2. (Color online) Contour plot of the total energy for a full spherical fully symmetric displacement of a (4,1) nanotube. The minima (bright yellow) are slightly displaced from the points (90°, 0°) and (90°, 180°) corresponding to outward and inward radial displacements, respectively.

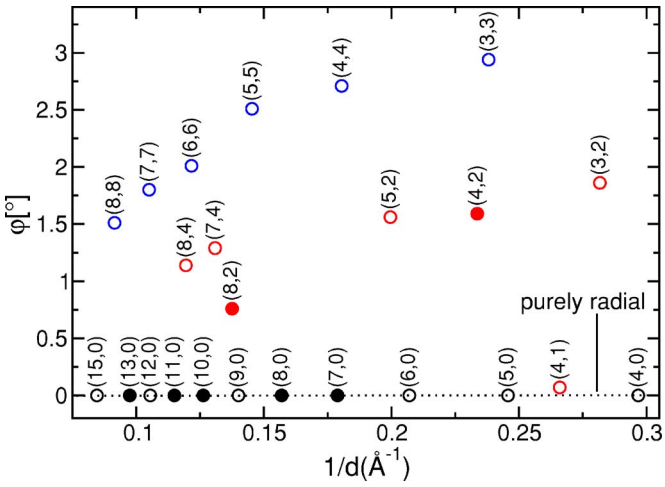

FIG. 3. (Color online) Angle φ as a function of the inverse nanotube diameter. We use the same symbols as in Fig. 1.

this minimum the eigenvector of the RBM. The values of ϑ and φ of the RBM eigenvector over the inverse NT diameter are shown in Figs. 1 and 3, respectively. As can be seen, the radial breathing mode has nonradial components irrespective of the chirality of the tube. These components become smaller as the diameter of the tube increases.

The achiral nanotubes have $\varphi=0°$ (zigzag NT) and $\vartheta=90°$ (armchair). This is due to their higher symmetry as compared to chiral nanotubes. Achiral tubes possess mirror planes, and therefore the fully symmetric representation A_1 of chiral NTs splits into the two representations A_{1g} and A_{1u}, even or odd under the mirror operation, respectively. Since armchair tubes possess a mirror plane perpendicular to the z axis and zigzag tubes possess a mirror plane that contains the z axis, the even A_{1g} mode cannot have components perpendicular to these planes. This symmetry restriction is the reason for the specific values of ϑ and φ of these tubes in Figs. 1 and 3 ($\vartheta=90°$ for armchair and $\varphi=0°$ for zigzag tubes).

The RBM of metallic zigzag tubes $[(n,0)$, n divisible by 3] shows a smaller nonradial component than that of semiconducting tubes of similar diameter. The nonradial component of metallic zigzag tubes shows an excellent agreement with the calculations of Dobardžić *et al.*,[5] whereas we obtain slightly larger nonradial components for semiconducting zigzag tubes. As the force constants in Ref. 5 were obtained from (semimetallic) graphite, differences between semiconducting and metallic tubes are not expected.

A simple model for the magnitude of the nonradial component of the eigenvector can be derived from considering the atomic forces in graphene. The nonradial component of the RBM compensates the nonradial forces caused by the bond stretching due to radial deformation. To simulate a purely radial vibration of a zigzag tube in graphene, we calculated the atomic forces after stretching the unit cell of graphene in zigzag direction. Due to graphene's symmetry, the resulting forces are perpendicular to the stretching direction and form a HEM-like pattern. We calculated the length of the HEM displacement necessary to compensate these forces. From a fit of these data, we obtain the normalized nonradial component of the RBM eigenvector $z_{\mathrm{RBM}}=\cos\theta$ of $(n,0)$ zigzag nanotubes,

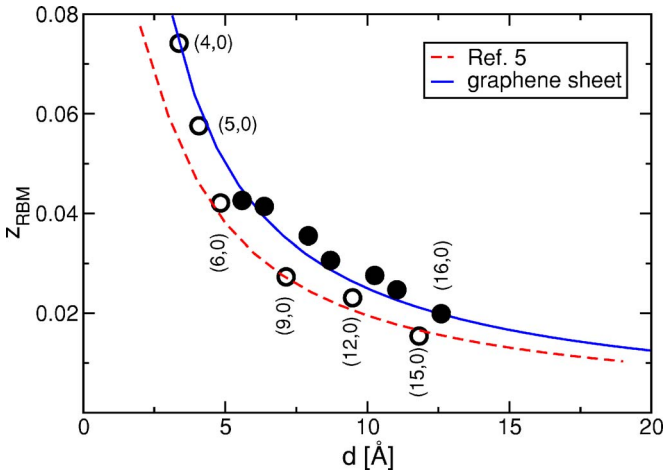

FIG. 4. (Color online) Normalized nonradial component of the RBM eigenvector z_{RBM} for zigzag NTs compared with that of Dobardžić *et al.* (Ref. 5) and our simple graphene model. The data of the metallic tubes fit well the model of Dobardžić *et al.*, whereas the semiconducting tubes show larger components. We use the same symbols as in Fig. 1.

$$z_{RBM} = \frac{2\pi}{19.7}\frac{1}{n}. \quad (1)$$

This is in good agreement with our data and the calculations of Dobardžić *et al.*,[5] as can be seen in Fig. 4. For larger tubes, where the effect of curvature becomes small, the agreement with Ref. 5 is excellent. This result can be extended to chiral tubes when multiplied with the factor $\cos(3\Theta)$, where Θ defines the chiral angle of the NT.

We have scanned the vicinity of the points ($\vartheta=0°$, $\varphi=0°$) and ($\vartheta=180°$, $\varphi=0°$) corresponding to the HEM displacement for selected zigzag NTs. We obtained the direction of maximal energy from a fit in the same way as for the RBM. The angular deviation from the z direction has a similar magnitude as the angular deviation of the RBM from the purely radial direction. This, as well as the results for the RBM, is in excellent agreement with finite-difference calculations of Refs. 8 and 18 that use the dynamical matrix for the calculation of phonon frequencies and eigenvectors. Therefore, in the next section, we calculate the eigenvector of the HEM using finite-difference calculations.

IV. FREQUENCY AND ELECTRON-PHONON COUPLING

We are interested in the influence of the small nonradial component on the phonon frequency and electron-phonon coupling strength. Experimentally, nanotubes are often identified via resonant Raman scattering of the diameter-dependent RBM and comparing the results with empirical data or theoretical predictions.[2] The squared magnitude of the electron-phonon interaction, $|\mathcal{M}_{e\text{-}ph}|^2$, among other factors, determines the Raman cross section and can be observed experimentally.[4,18,19] For small-chiral-angle tubes, $|\mathcal{M}_{e\text{-}ph}|^2$ can be 1 order of magnitude larger than that for armchair tubes.[8]

We calculated the RBM frequency in a frozen-phonon approach using the eigenvectors obtained in the previous section.[20] For comparison, we also calculated the frequencies for the purely radial displacement and found them to be overestimated by up to 10 cm^{-1}. This confirms the results of Milošević *et al.*[7] The frequencies of the eigenvectors are in excellent agreement with experiment and with *ab initio* finite-difference calculations.[8,21] A linear fit of our data $\omega_{RBM}=c_1/d+c_2$ leads to $c_1=2221$ Å cm^{-1} and $c_2=2$ cm^{-1}, in excellent agreement with other *ab initio* results, e.g., $c_1=2282$ Å cm^{-1} from Ref. 22 or $c_1=2340$ Å cm^{-1} from Ref. 6, or experimental data $c_1=2150$ Å cm^{-1} and $c_2=18$ cm^{-1} from Ref. 21. So for accurate frequency calculations, the RBM may not be approximated as a purely radial displacement.

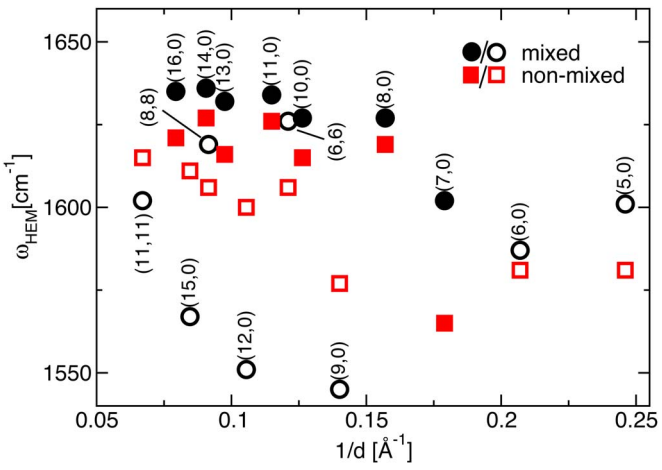

FIG. 5. (Color online) Frequency ω_{HEM} from finite-difference calculation including mixing (circles) and for the nonmixed frozen-phonon calculation (squares). Open (closed) symbols denote metallic (semiconducting) NTs. Frequencies of the nonmixed modes are underestimated, except for most metallic zigzag tubes.

Similarly, we calculated the frequencies of the Raman-active HEM for the nonmixed displacement, strictly perpendicular to the radial direction. The fully symmetric HEM is not purely axial or not purely circumferential in zigzag and armchair tubes, respectively, and the mixing influences the phonon frequencies. We compare these to frequencies from finite-difference calculations that include mixing with the RBM in Fig. 5.[18] In both cases, we find softening of the HEM frequency for metallic tubes, as well established in literature.[9,23] The change in frequency due to the mixing is also different for metallic and semiconducting tubes: For semiconducting NTs, the results differ by up to 20 cm^{-1}. In metallic NTs, the difference is as high as 50 cm^{-1} in the opposite direction: the frequencies are higher if no mixing is allowed.

Now we concentrate on the effect of the mixing on electron-phonon coupling strengths. The deformation potential $\partial E_{\mathbf{k}n}/\partial Q_\alpha$ for the nonmixed displacement patterns was obtained in a frozen-phonon approach as described in Ref. 8. From the deformation potentials, the matrix elements $\mathcal{M}_{e\text{-}ph}^{\alpha,\mathbf{k}n}$ were obtained (same notations used as in Ref. 8). We find an increase of $\partial E_{\mathbf{k}n}/\partial Q_\alpha$ and of the matrix elements for the radial displacement pattern between 30% and 60% with respect to the results of Ref. 8, which include the mixing. This is of special interest as the intensity observed in Raman ex-

TABLE I. Relative error of the matrix elements for the nonmixed radial displacement of the RBM compared to the results of Ref. 8. The mixed eigenvectors predict systematically smaller matrix elements than the simplified (nonmixed) ones.

NT	$\mathcal{M}_1$	$\mathcal{M}_2$	$\mathcal{M}_3$	$\mathcal{M}_4$
(10,0)	1.43	1.58	1.46	1.46
(6,6)	1.36			
(8,4)	1.34		1.34	
(8,8)	1.37	1.36	1.36	
(14,0)	1.51	1.46	1.48	
(15,0)	1.27	1.35	1.32	1.25
(16,0)	1.45	1.51	1.47	
(11,11)	1.31	1.36	1.37	

periments is proportional to the square of $\mathcal{M}_{e\text{-}ph}^{\alpha,\mathbf{k}n}$. The mixed eigenvectors thus yield systematically smaller Raman signals than the assumption of a purely radial mode would suggest. The change of $\partial E_{\mathbf{k}n}/\partial Q_\alpha$ depends on chirality and conduction character. In Table I, we show the relative increase compared to the values of the mixed eigenvectors in Ref. 8. For semiconducting zigzag tubes, the average of the matrix elements increases by a factor of 1.5, whereas for metallic zigzag tubes (15,0), we find an increase of 30%. For armchair tubes, we find an increase of 1.3–1.4.

The matrix elements of the RBM are diminished by the mixing for all NTs. This is surprising, since the relative sign of $\mathcal{M}_i^{\mathrm{HEM}}$ and $\mathcal{M}_i^{\mathrm{RBM}}$ depends on chirality (see Ref. 24). The relative orientation of the HEM- and RBM-like components in an eigenvector is, however, also chirality dependent. We illustrate this in Fig. 6. In zigzag nanotubes, when the radial component points outward, the bonds parallel to the axis are elongated. In armchair tubes, the equivalent bonds that are perpendicular to the axis are shortened instead. The different orientation of both components compensates the difference in sign of the matrix elements, yielding the same trend for all NTs.

In contrast to the RBM, the mixing of the HEMs only little influences their deformation potentials. The deformation potentials of the nonmixed HEM do not show any detectable difference for zigzag tubes; for armchair tubes, we find an increase of the matrix elements of 4%–7% for the nonmixed modes compared to the results in Ref. 18, which include the mixing. The small influence of the mixing on the deformation potential is due to the low electron-phonon coupling strength of the RBM relative to the HEM.

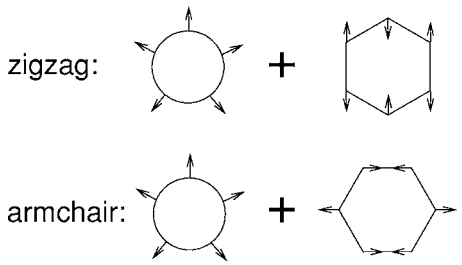

FIG. 6. Figure illustrating the mixing between the radial and the tangential components of the RBM in zigzag and armchair tubes when the radial component points outward.

V. CONCLUSION

We presented a detailed study of the mixing of the fully symmetric Raman-active modes in carbon nanotubes. We confirmed via an independent variational approach that the RBM has small nonradial components. They have only little influence on phonon frequency calculations but a big quantitative effect on electron-phonon coupling matrix element $\mathcal{M}_{e\text{-}ph}$ with changes of up to 60%. In analogy, the HEM is not purely axial or circumferential. Here, we find a big influence of the mixing on the phonon frequency calculation but a rather small effect on the magnitude of $\mathcal{M}_{e\text{-}ph}$. Our results have important implications for the determination of chiral abundances in ensembles of nanotubes, when obtained via the Raman-scattering strength of nanotubes of different chiralities.

ACKNOWLEDGMENT

The authors acknowledge useful discussions with J. Maultzsch.

*Electronic address: marcel@physik.tu-berlin.de

[1] S. M. Bachilo, M. S. Strano, C. Kittrel, R. H. Hauge, R. E. Smalley, and R. B. Weisman, Science **298**, 2361 (2002).
[2] H. Telg, J. Maultzsch, S. Reich, F. Hennrich, and C. Thomsen, Phys. Rev. Lett. **93**, 177401 (2004).
[3] H. M. Lawler, D. Areshkin, J. W. Mintmire, and C. T. White, Phys. Rev. B **72**, 233403 (2005).
[4] S. V. Goupalov, Phys. Rev. B **71**, 153404 (2005).
[5] E. Dobardžić, I. Milošević, B. Nikolić, T. Vuković, and M. Damnjanović, Phys. Rev. B **68**, 045408 (2003).
[6] J. Kürti, V. Zólyomi, M. Kertesz, and G. Sun, New J. Phys. **5**, 125 (2003).
[7] I. Milošević, E. Dobardžić, and M. Damnjanović, Phys. Rev. B **72**, 085426 (2005).
[8] M. Machón, S. Reich, H. Telg, J. Maultzsch, P. Ordejón, and C. Thomsen, Phys. Rev. B **71**, 035416 (2005).
[9] O. Dubay and G. Kresse, Phys. Rev. B **67**, 035401 (2003).
[10] M. Damnjanović, E. Dobardžić, and I. Milošević, J. Phys.: Condens. Matter **16**, L505 (2004).
[11] G. Sun, J. Kürti, P. Rajczy, M. Kertesz, J. Hafner, and G. Kresse, J. Mol. Struct.: THEOCHEM **624**, 37 (2003).
[12] M. Damnjanović, I. Milošević, T. Vuković, and R. Sredanović, Phys. Rev. B **60**, 2728 (1999).
[13] P. Ordejón, E. Artacho, and J. M. Soler, Phys. Rev. B **53**, R10441 (1996).
[14] J. M. Soler, E. Artacho, J. D. Gale, A. García, J. Junquera, P. Ordejón, and D. Sánchez-Portal, J. Phys.: Condens. Matter **14**, 2745 (2002).
[15] J. P. Perdew and A. Zunger, Phys. Rev. B **23**, 5048 (1981).
[16] N. Troullier and J. L. Martins, Phys. Rev. B **43**, 1993 (1991).

[17] H. J. Monkhorst and J. D. Pack, Phys. Rev. B **13**, 5188 (1976).
[18] M. Machón, S. Reich, and C. Thomsen, Phys. Rev. B **74**, 205423 (2006).
[19] Z. Luo, F. Papadimitrakopoulos, and S. K. Doorn, Appl. Phys. Lett. **88**, 073110 (2006).
[20] M. T. Yin and M. L. Cohen, Phys. Rev. B **26**, 3259 (1982).
[21] J. Maultzsch, H. Telg, S. Reich, and C. Thomsen, Phys. Rev. B **72**, 205438 (2005).
[22] V. N. Popov and P. Lambin, Phys. Rev. B **73**, 085407 (2006).
[23] J. Kürti, V. Zólyomi, M. Kertesz, G. Sun, R. H. Baughman, and H. Kuzmany, Carbon **42**, 971 (2004).
[24] M. Machón, S. Reich, and C. Thomsen, Phys. Status Solidi B **243**, 3166 (2006).